Accelerometer Calibration and Dynamic Bias and Gravity Estimation: Analysis, Design, and Experimental Evaluation

Pedro Batista, *Student Member, IEEE*, Carlos Silvestre, *Member, IEEE*, Paulo Oliveira, *Member, IEEE*, and Bruno Cardeira

***Abstract*—Tri-axial linear accelerometers are key components in a great variety of applications and, in particular, in navigation systems. Nonidealities such as scale factors, cross coupling, bias, and other higher-order nonlinearities affect the output of this sensor, leading, in general, to prohibitive errors. On the other hand, these coefficients are often slowly time-varying, which renders offline calibration less effective. One such coefficient that usually varies greatly over time and between power-ons is the bias. This paper details the calibration of an accelerometer unit and presents also a dynamic filtering solution for the bias, which also includes the estimation of the gravity in body-fixed coordinates. Simulation and experimental results obtained with a motion rate table are presented and discussed to illustrate the performance of the proposed algorithms.**

***Index Terms*— Accelerometers, calibration, Kalman filters, navigation, sensor systems and applications.**

I. Introduction

RECENT advances in materials and production processes have led to the increasingly miniaturization of a large variety of sensing devices. Among these sensors are a new generation of micro-electro-mechanical systems (MEMS) accelerometers, which are nowadays used in a large variety of applications. These sensors have good dynamic specifications, considering the cost, size, and power requirements, but are often subject to large offsets, cross-coupling factors, and other nonlinearities. While in some cases these nonidealities are of no importance, e.g., in cell phones to detect the vertical direction or in computer hardware for active hard drive protection, they are prohibitive for the design of navigation systems, which justifies offline calibration. Furthermore, the coefficients of these nonidealities are often slowly time-varying, which renders offline calibration less effective and substantiates the need for online parameter estimation. This paper presents the calibration of a low-cost tri-axial accelerometer and a novel filtering solution for online bias and gravity estimation with application to the design of navigation systems for mobile platforms.

High performance accelerometers are a key element and have been extensively used in Inertial Navigation Systems (INS). With the widespread use of MEMS technology, accelerometers are nowadays a fundamental aiding sensor for attitude estimation in low-cost, middle range performance Attitude and Heading Reference Systems (AHRS), with application to autonomous air, ground, and ocean robots. These inexpensive, low power sensors, used as pendula, allow for accurate attitude estimates at very low frequency by comparing the Earth gravitational field vector measurements in body frame coordinates with the vertical, see [1], [2], and references therein for examples of such application in attitude estimation. The integration of accelerometer readings with Global Positioning System (GPS) measurements are commonly employed for linear motion estimation in Integrated Navigation Systems, see [3] and references therein for examples of such application.

The topic of accelerometer calibration has been subject of intensive research. Indeed, various methods have been proposed in the literature, from precision centrifuge tests of linear accelerometers [4] to multi-position methods [5]–[7]. In [8], error models for inertial sensors, including a solid-state tri-axial accelerometer, were explicitly included in an extended Kalman filter (EKF) to estimate the position and orientation of a robot, while in [9] Kalman filtering techniques were applied to the calibration and alignment of Inertial Navigation Systems, which was also studied in [10]. More recently, in [11], nonlinear Kalman filters, of first and second order, coupled with position feedback, were used to characterize accelerometers. An optimization-based calibration procedure for tri-axial accelerometer-magnetometers was proposed in [12], where a robotic arm is used to generate different angular positions of the body of the sensor. In [13] a fully electrical setup was proposed to test and calibrate MEMS accelerometers and a case study was presented in [14], where a 4-DOF system is proposed for fully automated accelerometer calibration. An interesting survey on the history of accelerometers, which also includes a section on calibration activities, is found in [15].

The contribution of this paper is twofold: 1) an accelerometer calibration technique is proposed and applied to offline

Manuscript received January 21, 2010; revised April 27, 2010; accepted July 10, 2010. Manuscript received in final form September 06, 2010. Recommended by Associate Editor A. Alessandri. The work of P. Batista was supported by a Ph.D. Student Scholarship with reference SFRH/BD/24862/2005 from Fundação para a Ciência e a Tecnologia. This work was supported in part by Fundação para a Ciência e a Tecnologia (ISR/IST plurianual funding) through the PIDDAC Program funds, by the Projects PTDC/EEAACR/72853/2006 HELICIM and PTDC/MAR/64546/2006-OBSERVFLY of the FCT, and by the AIRTICI Project from AdI.

The authors are with the Institute for Systems and Robotics, Instituto Superior Técnico (IST), 1049-001 Lisboa, Portugal (e-mail: pbatista@isr.ist.utl.pt; cjs@isr.ist.utl.pt; pjcro@isr.ist.utl.pt; bcardeira@isr.ist.utl.pt).

accelerometer calibration that includes the estimation of bias, scale factors, cross coupling factors, and quadratic coefficients and 2) a time-varying Kalman filter is derived for online dynamic bias and gravity estimation. The calibration technique proposed in the paper resorts to attitude relative measurements as provided by a Motion Rate Table (MRT). The *a priori* knowledge of the gravity vector is not required since it is also explicitly estimated, in contrast with previous methods that assume that the vertical is known. The second part of this paper is of particular importance for the design of navigation systems since it allows for online estimation of the accelerometer bias which, for low-cost units, is usually time-varying, rendering offline calibration less effective. Moreover, the gravity is also estimated, in body-fixed coordinates. This is in contrast with previous solutions where the gravitational term is canceled resorting to the knowledge of the attitude of the body, therefore leading to cancellation problems that cause a severe degradation in the performance of the resulting navigation systems. In addition to simulation results, the proposed algorithms were experimentally evaluated resorting to a motion rate table, which offers ground truth data.

This paper is organized as follows. The accelerometer models are presented and discussed in Section II. Section III details the offline calibration technique proposed in the paper, while the online dynamic bias and gravity estimation solution is derived in Section IV. Simulation and experimental results are given in Sections V and VI, respectively, including both the offline calibration of a low-cost MEMS accelerometer and dynamic bias and gravity estimation tests. Finally, Section VII summarizes the main conclusions and contributions of this paper.

A. Notation

Throughout this paper the symbol $\mathbf{0}$ denotes a matrix of zeros and $\mathbf{I}$ the identity matrix, both of appropriate dimensions, while $\mathrm{diag}(\mathbf{A}_1, \ldots, \mathbf{A}_n)$ is a block diagonal matrix. If $\mathbf{x} \in \mathbb{R}^3$ and $\mathbf{y} \in \mathbb{R}^3$ are two vectors, $\mathbf{x} \times \mathbf{y}$ represents the cross product. For $\mathbf{x} = [x_1 \ldots x_n]^T \in \mathbb{R}^n$, the vector $\boldsymbol{x}^i$ is defined as the vector that results from the element-wise power operation, i.e., $\mathbf{x}^i := [x_1^i \ldots x_n^i]^T \in \mathbb{R}^n$, while the vector $\boldsymbol{x}^{|i|}$ is defined as

$$\boldsymbol{x}^{|i|} := \begin{bmatrix} \mathrm{sign}(\mathrm{x_1})\mathrm{x_1^i} \\ \vdots \\ \mathrm{sign}(\mathrm{x_n})\mathrm{x_n^i} \end{bmatrix}.$$

The rotation matrix from a coordinate frame $\{A\}$ to a coordinate frame $\{B\}$ is denoted by ${}^B_A\mathbf{R}$. Finally, the Dirac delta function is denoted by $\delta(t)$.

II. Accelerometer Model

The simplest accelerometer model for single axis sensors considers only a scale factor and a constant offset, as given by

$$a_m(t) = fa(t) + b$$

where $a_m(t)$ is the output of the accelerometer, f is the scale factor, b denotes the bias, and $a(t)$ stands for the acceleration that is measured in the absence of offsets, which includes not only the acceleration of the body of the accelerometer but also a term due to the effect of the gravitational field on the mass whose acceleration is actually measured, which is not coincident with the accelerometer case. Notice that the term due to the gravitational field appears regardless of the accelerometer technology as all objects are subject to the gravitational force, which induces a force of opposite direction to the gravity on the mass whose acceleration is actually measured, see [5] and [16] for further details.

For navigation purposes, tri-axial accelerometers, composed of three, single-axis, orthogonally mounted linear accelerometers, are employed. The generalization of the simplest single-axis model for tri-axial accelerometers, which accounts for scale factors and bias, reads as

$$\mathbf{a}_m(t) = \mathbf{F}\mathbf{a}(t) + \mathbf{b} \tag{1}$$

where $\mathbf{F} \in \mathbb{R}^{3\times3}$ is a diagonal matrix that includes the scale factors, $\mathbf{b} \in \mathbb{R}^3$ is the bias, and

$$\mathbf{a}(t) = \dot{\mathbf{v}}(t) + \mathbf{S}\left[\boldsymbol{\omega}(t)\right]\boldsymbol{v}(t) - \boldsymbol{g}(t)$$

where $\mathbf{v}(t)$ and $\boldsymbol{\omega}(t)$ denote the linear and angular velocities of the body-fixed frame $\{B\}$, respectively, expressed in body-frame coordinates, $\mathbf{S}[\boldsymbol{\omega}(t)] \in \mathbb{R}^{3\times3}$ is the skew symmetric matrix such that $\mathbf{S}[\boldsymbol{\omega}(t)]\mathbf{v}(t) = \boldsymbol{\omega}(t) \times \mathbf{v}(t)$, and $\mathbf{g}(t) \in \mathbb{R}^3$ is the acceleration of gravity, expressed in body-fixed coordinates. In practice, the set of single-axis accelerometers is not orthogonally mounted, which introduces cross coupling between the acceleration felt on the different accelerometer axes. This non-ideality may be simply modeled by no longer considering $\mathbf{F}$ as a diagonal matrix. Instead, $\mathbf{F}$ is just assumed to be an invertible matrix, which accounts simultaneously, in this case, for scale and cross coupling factors.

The accelerometer model (1) is still, and in spite of capturing already a different number of nonidealities, only an approximation of the real model. Indeed, the electrical devices involved in the measurement process, from transducers to amplifiers, are not linear, do not have constant coefficients, and are subject to different types of noise. A more complete (and complex) model [4], that includes higher-order terms, is given by

$$\begin{aligned}\mathbf{a}_m(t) = \mathbf{F}\mathbf{a}(t) + \mathbf{b} + \mathbf{F}\mathbf{F}_2\mathbf{a}^2(t) + \mathbf{F}\mathbf{F}_{|2|}\mathbf{a}^{|2|}(t) \\ + \mathbf{F}\mathbf{F}_3\mathbf{a}^3(t) + \mathbf{F}\mathbf{F}_{|3|}\mathbf{a}^{|3|}(t) + \ldots\end{aligned}$$

where $\mathbf{F}_2 \in \mathbb{R}^{3\times3}$, $\mathbf{F}_{|2|} \in \mathbb{R}^{3\times3}$, $\mathbf{F}_3 \in \mathbb{R}^{3\times3}$, and $\mathbf{F}_{|3|} \in \mathbb{R}^{3\times3}$ are diagonal matrices.

Nonlinear time-varying models for accelerometers, with many parameters, offer better accuracies, at the expense of the complexity. From the practical point of view, it seems appealing to use simpler methods that preserve accuracy as: 1) for very highly nonlinear time-varying dynamic models the complexity of the inversion of the model could be overwhelming. Closed-form solutions are obviously not available and iterative numerical solvers would be required to operate in real-time; 2) time-varying models would be likely to depend on other variables such as temperature, which would require additional sensors; and 3) the effect of higher-order nonlinearities is often very mild, particularly when compared to the magnitude of the electrical noise. Therefore, the model employed in this

work, and after successful experimental validation of the model accuracy, is

$$\mathbf{a}_m(t) = \mathbf{F}\left[\mathbf{a}(t) + \mathbf{F}_2\mathbf{a}^2(t)\right] + \mathbf{b} + \mathbf{n}_a(t) \tag{2}$$

where $\mathbf{n}_a(t)$ denotes the accelerometer noise. The quadratic even term was chosen as it was evident, from experimental evaluation, that this was the most dominant nonlinear term. Moreover, there exists a closed-form solution to obtain $\mathbf{a}(t)$ from (2), which is a precious advantage for real-time navigation applications since no iterative solvers are required.

III. Accelerometer Offline Calibration

There exists a multitude of tests and calibration procedures described in the literature. In this paper it is assumed that the accelerometer is exposed to several different known rotations and a rather large number of measurements is taken at each static position. This can be achieved resorting to a tri-axial motion rate table, e.g., the Ideal Aerosmith Model 2103HT, used in this work to obtain the experimental data.

The motion rate table outputs the rotation from body-fixed to inertial coordinates apart from an installation error due to non-horizontal mounting of the table. If there is a precision level available, this installation error is known and it is possible to compute the rotation matrix $\mathbf{R}$ from body-fixed to inertial coordinates. Otherwise, it is necessary to consider

$$\mathbf{R}(t) = {}^I_T\mathbf{R}\,{}^T_B\mathbf{R}(t)$$

where ${}^T_B\mathbf{R}(t)$ is the rotation from body-fixed coordinates to the table installation fixed reference frame, which is given by the calibration table, and ${}^I_T\mathbf{R}$ corresponds to the matrix that encodes the installation offset.

Since measurements are considered only at static positions, it is true that

$$\mathbf{v}(t) = \dot{\mathbf{v}}(t) = \mathbf{0}.$$

Therefore, using (2), the nominal accelerometer readings are given by

$$\mathbf{a}_m(t) = \mathbf{F}\left[-\mathbf{g}(t) + \mathbf{F}_2\mathbf{g}^2(t)\right] + \mathbf{b}. \tag{3}$$

The acceleration of gravity in body-fixed coordinates may be expressed as

$$\mathbf{g}(t) = \mathbf{R}^T(t)\,{}^I\mathbf{g}$$

where ${}^I\mathbf{g}$ is the acceleration of gravity expressed in inertial coordinates. Nowadays, there exist very accurate models for the acceleration of the gravity, e.g., the 1984 World Geodetic System (WGS84), see [17] for further details. Therefore, if $\mathbf{R}$ is known, the computation of $\mathbf{F}$, $\mathbf{F}_2$, and $\mathbf{b}$ corresponds to the simple determination of linear coefficients. In the case considered in the paper only ${}^T_B\mathbf{R}$ is known, which means that the direction of the gravity must also be determined. In this case, it is possible to rewrite (3) as

$$\mathbf{a}_m(t) = \mathbf{F}\left(-{}^T_B\mathbf{R}^T(t)\,{}^T\mathbf{g} + \mathbf{F}_2\left[{}^T_B\mathbf{R}^T(t)\,{}^T\mathbf{g}\right]^2\right) + \mathbf{b} \tag{4}$$

where

$${}^T\mathbf{g} = {}^I_T\mathbf{R}^T\,{}^I\mathbf{g}$$

is the acceleration of gravity expressed in table-fixed coordinates. Multiplying (4) on the left by $\mathbf{F}^{-1}$ gives

$$\mathbf{F}^{-1}\mathbf{a}_m(t) + {}^T_B\mathbf{R}^T(t)\,{}^T\mathbf{g} - \mathbf{F}_2\left[{}^T_B\mathbf{R}^T(t)\,{}^T\mathbf{g}\right]^2 - \mathbf{b}' = \mathbf{0} \tag{5}$$

where

$$\mathbf{b}' = \mathbf{F}^{-1}\mathbf{b}.$$

Equation (5) presents a better form than (4) in order to estimate the unknown parameters $\mathbf{F}$, $\mathbf{b}$, $\mathbf{F}_2$, and the acceleration of gravity in table coordinates, ${}^T\mathbf{g}$, since it has less products between unknowns. Nevertheless, a quadratic term still exists. In the presence of noise, there is no exact solution to (5) if a large set of measurements is considered. A simple and computationally efficient way to calibrate the accelerometer is to solve an optimization problem in two steps. First, the quadratic term is ignored, which allows to write, for a set of static measurements $\{\mathbf{a}_m(t_i), i = 1, \ldots, N\}$, corresponding to a set of rotation matrices $\{{}^T_B\mathbf{R}(t_i), i = 1, \ldots, N\}$

$$\begin{bmatrix}\mathbf{D}_a(t_i) & {}^T_B\mathbf{R}^T(t_i) & -\mathbf{I}\end{bmatrix}\begin{bmatrix}\mathbf{f}\\ {}^T\mathbf{g}\\ \mathbf{b}\end{bmatrix} = \mathbf{0}$$

where

$$\mathbf{D}_a(t) = \begin{bmatrix}\mathbf{a}_m^T(t) & \mathbf{0} & \mathbf{0}\\ \mathbf{0} & \mathbf{a}_m^T(t) & \mathbf{0}\\ \mathbf{0} & \mathbf{0} & \mathbf{a}_m^T(t)\end{bmatrix} \in \mathbb{R}^{3\times 9}$$

and

$$\mathbf{f} = \begin{bmatrix}\mathbf{f}_1\\ \mathbf{f}_2\\ \mathbf{f}_3\end{bmatrix} \in \mathbb{R}^9, \quad \mathbf{F}^{-1} = \begin{bmatrix}\mathbf{f}_1^T\\ \mathbf{f}_2^T\\ \mathbf{f}_3^T\end{bmatrix}.$$

Define the stack matrix $\mathbf{X}$ as

$$\mathbf{X} = \begin{bmatrix}\mathbf{D}_a(t_1) & {}^T_B\mathbf{R}^T(t_1) & -\mathbf{I}\\ \mathbf{D}_a(t_2) & {}^T_B\mathbf{R}^T(t_2) & -\mathbf{I}\\ \vdots & \vdots & \vdots\\ \mathbf{D}_a(t_N) & {}^T_B\mathbf{R}^T(t_N) & -\mathbf{I}\end{bmatrix}.$$

In the presence of sensor noise, a simple solution corresponds to the minimization problem

$$\mathbf{x}_o = \arg\min_{||\mathbf{x}_o||=1} ||\mathbf{X}\mathbf{x}_o||$$

which is easily obtained from the vector associated with the minimum singular value of the singular value decomposition (SVD) of $\mathbf{X}$. The magnitude of the acceleration of gravity, as

TABLE I
ALGORITHM TO CALIBRATE THE ACCELEROMETER

1) Compute the SVD of $\mathbf{X}$. Select the vector associated with the minimum singular value.
2) Normalize the SVD solution obtained in Step 1 according to the magnitude of the gravity and its direction (sign of the z-coordinate).
3) Use the gravity estimate obtained in Step 2 and compute the SVD of $\mathbf{X}_2$. Select the vector associated with the minimum singular value.
4) Normalize the SVD solution obtained in Step 3 according to the magnitude of the gravity and its direction (sign of the z-coordinate).
5) Use the current gravity estimate in $\mathbf{X}_2$ and go to Step 3. Stop once the difference between the previous gravity estimate and the most recent goes below a predefined threshold.

well as its direction, are used to normalize the resulting SVD solution.

The solution of this first step, in particular the gravity vector, is used as an estimate for the quadratic term in (5), which allows to also consider (5) as linear in the parameters, with

$$\left[\mathbf{D}_a(t_i)\ {}^{T}_{B}\mathbf{R}^{T}(t_i)\ -\mathrm{diag}\left(\left[{}^{\mathrm{T}}_{\mathrm{B}}\mathbf{R}^{\mathrm{T}}(\mathrm{t_i})\ {}^{\mathrm{T}}\hat{\mathbf{g}}\right]^2\right)\ -\mathbf{I}\right]\begin{bmatrix}\mathbf{f}\\ {}^{T}\mathbf{g}\\ \mathbf{f}_2\\ \mathbf{b}\end{bmatrix}=\mathbf{0}$$

where $\mathbf{f}_2 \in \mathbb{R}^3$ is the vector that contains the diagonal elements of the diagonal matrix $\mathbf{F}_2$ and ${}^{T}\hat{\mathbf{g}}$ is the estimate of the gravity vector previously obtained. Stacking all observations gives

$$\mathbf{X}_2\begin{bmatrix}\mathbf{f}\\ {}^{T}\mathbf{g}\\ \mathbf{f}_2\\ \mathbf{b}\end{bmatrix}=\mathbf{0}$$

with

$$\mathbf{X}_2=\begin{bmatrix}\mathbf{D}_a(t_1) & {}^{T}_{B}\mathbf{R}^{T}(t_1) & -\mathrm{diag}\left(\left[{}^{\mathrm{T}}_{\mathrm{B}}\mathbf{R}^{\mathrm{T}}(\mathrm{t_1})^{\mathrm{T}}\hat{\mathbf{g}}\right]^2\right) & -\mathbf{I}\\ \mathbf{D}_a(t_2) & {}^{T}_{B}\mathbf{R}^{T}(t_2) & -\mathrm{diag}\left(\left[{}^{\mathrm{T}}_{\mathrm{B}}\mathbf{R}^{\mathrm{T}}(\mathrm{t_2})^{\mathrm{T}}\hat{\mathbf{g}}\right]^2\right) & -\mathbf{I}\\ \vdots & \vdots & \vdots & \\ \mathbf{D}_a(t_N) & {}^{T}_{B}\mathbf{R}^{T}(t_N) & -\mathrm{diag}\left(\left[{}^{\mathrm{T}}_{\mathrm{B}}\mathbf{R}^{\mathrm{T}}(\mathrm{t_N})^{\mathrm{T}}\hat{\mathbf{g}}\right]^2\right) & -\mathbf{I}\end{bmatrix}.$$

The parameters are readily obtained by computing the vector associated with the minimum singular value of $\mathbf{X}_2$ and normalizing it according to the known magnitude of the gravity. Finally, it is possible to reiterate this last step using as new gravity estimate the solution of each previous step. The proposed algorithm is detailed in Table I.

IV. DYNAMIC BIAS AND GRAVITY ESTIMATION

Although theoretically possible for certain maneuvers, online estimation of the parameters of the accelerometer model (2) is not practical: the number of unknown coefficients is too large and highly aggressive maneuvers would be required to achieve only a moderate level of performance. However, it is important to include, in navigation systems, a simplified model to account for some of the nonidealities of the accelerometers. The simplest of these is the sensor bias, and while it is only one constant for each axis, it is well known that an offset in the acceleration measurement results in a severe degradation of the performance of the navigation solutions. Furthermore, experimental results evidence that the bias varies greatly, not only over time but also between power-ons.

It was shown in [18] that, assuming that the accelerometer has been previously calibrated, removing the effect of scale and cross factor errors and ignoring higher-order nonlinearities, the bias may be estimated under some mild assumptions. Therefore, it is assumed in this section that the accelerometer has been previously calibrated using the technique proposed in the previous section, which allows to use the model

$$\mathbf{a}_m(t)=\dot{\mathbf{v}}(t)+\mathbf{S}\left[\boldsymbol{\omega}(t)\right]\mathbf{v}(t)-\mathbf{g}(t)+\mathbf{b}+\mathbf{n}_a(t). \quad (6)$$

The acceleration of gravity $\mathbf{g}$ (in body-fixed coordinates) is not known in robotic applications. While there are models for its magnitude, its direction depends on the attitude of the robot, and it is used, in fact, to estimate this variable. A common assumption when designing attitude filters is that the magnitude of the acceleration of gravity dominates, for sufficiently low frequencies, the other terms, see [1] for an example of such application. The direction of the gravity is approximated, in that case, by

$$\mathbf{d}_{\mathbf{g}}(t)\approx\frac{\mathbf{a}_m(t)}{||\mathbf{a}_m(t)||}$$

which induces errors in the attitude estimates. While these errors are in general negligible, they may prove to be prohibitive for highly maneuvering vehicles, e.g., aerial robots, vehicles executing trajectories with approximately constant accelerations, or applications where high-accuracy requirements are in place, such as space applications. Therefore, the gravity acceleration in body-coordinates is also considered as an unknown in this framework.

The direction of the acceleration of gravity is locally constant in inertial coordinates. Therefore, the time derivative of $\mathbf{g}$ is simply given by

$$\dot{\mathbf{g}}(t)=-\mathbf{S}\left[\boldsymbol{\omega}(t)\right]\mathbf{g}(t).$$

The bias, later assumed to correspond to a random walk process is, at this point, assumed to be constant, which means that

$$\dot{\mathbf{b}}(t)=\mathbf{0}.$$

Finally, from (6), it is possible to write

$$\dot{\mathbf{v}}(t)=\mathbf{a}_m(t)-\mathbf{S}\left[\boldsymbol{\omega}(t)\right]\mathbf{v}(t)+\mathbf{g}(t)-\mathbf{b}-\mathbf{n}_a(t).$$

In this work it is assumed that linear velocity readings are available in order to estimate $\mathbf{b}$ and $\mathbf{g}$. Nevertheless, extending the framework to also estimate $\mathbf{v}$ considering linear position measurements is trivial, see [18] for further details. The final system dynamics, considering state disturbances and measurement noise, are given by

$$\begin{cases}\dot{\mathbf{x}}(t)=\mathbf{A}(t)\mathbf{x}(t)+\mathbf{B}\mathbf{a}_m(t)+\mathbf{n}_x(t)\\ \mathbf{y}(t)=\mathbf{C}\mathbf{x}(t)+\mathbf{n}_y(t)\end{cases} \quad (7)$$

where $\mathbf{x}(t)=\left[\mathbf{v}^T(t)\mathbf{g}^T(t)\mathbf{b}^T(t)\right]^T$ is the system state

$$\mathbf{A}(t) = \begin{bmatrix} -\mathbf{S}[\boldsymbol{\omega}(t)] & \mathbf{I} & -\mathbf{I} \\ \mathbf{0} & -\mathbf{S}[\boldsymbol{\omega}(t)] & \mathbf{0} \\ \mathbf{0} & \mathbf{0} & \mathbf{0} \end{bmatrix}$$

$$\mathbf{B} = \begin{bmatrix} \mathbf{I} \\ \mathbf{0} \\ \mathbf{0} \end{bmatrix}$$

$\mathbf{C} = [\mathbf{I}\,\mathbf{0}\,\mathbf{0}]$, and $\mathbf{n}_x$ and $\mathbf{n}_y$ are assumed to be zero-mean white Gaussian noise, with

$$\begin{aligned} \mathrm{E}\left[\mathbf{n}_{\mathrm{x}}(\mathrm{t}_1)\mathbf{n}_{\mathrm{x}}^{\mathrm{T}}(\mathrm{t}_2)\right] &= \boldsymbol{\Xi}(\mathrm{t})\delta(\mathrm{t}_1 - \mathrm{t}_2), \\ \mathrm{E}\left[\mathbf{n}_{\mathrm{y}}(\mathrm{t}_1)\mathbf{n}_{\mathrm{y}}^{\mathrm{T}}(\mathrm{t}_2)\right] &= \boldsymbol{\Theta}(\mathrm{t})\delta(\mathrm{t}_1 - \mathrm{t}_2) \end{aligned}$$

and

$$\mathrm{E}\left[\mathbf{n}_{\mathrm{x}}(\mathrm{t}_1)\mathbf{n}_{\mathrm{y}}^{\mathrm{T}}(\mathrm{t}_2)\right] = \mathbf{0}$$

where $\boldsymbol{\Xi}$ and $\boldsymbol{\Theta}$ are the process and noise intensity matrices, respectively. The linear time-varying system (7) is observable on $[t_0, t_f]$ if and only if the direction of the angular velocity $\boldsymbol{\omega}(t)$ changes for some $t_1 \in [t_0, t_f]$ or, equivalently

$$\begin{aligned} \forall\, \exists : \mathbf{S}[\boldsymbol{\omega}(t_1)]\,\mathbf{d} \neq \mathbf{0}. \\ \mathbf{d} \in \mathbb{R}^3 \quad t_1 \in [t_0, t_f] \\ ||\mathbf{d}|| = 1. \end{aligned}$$

The proof of this result can be found in [18]. Therefore, the estimation problem is well-posed and the time-varying Kalman filter design is straightforward, see [19] and [20]. For the sake of completeness, the Kalman filter equations are given by

$$\dot{\hat{\mathbf{x}}}(t) = \mathbf{A}(t)\hat{\mathbf{x}}(t) + \mathbf{K}(t)\left[\mathbf{y}(t) - \mathbf{C}\hat{\mathbf{x}}(t)\right]$$

for the state estimate, while the covariance matrix evolves according to

$$\dot{\mathbf{P}}(t) = \mathbf{A}(t)\mathbf{P}(t) + \mathbf{P}(t)\mathbf{A}^T(t) + \boldsymbol{\Xi}(t) - \mathbf{P}(t)\mathbf{C}^T\boldsymbol{\Theta}^{-1}\mathbf{C}\mathbf{P}(t).$$

The Kalman gain matrix is given by

$$\mathbf{K}(t) = \mathbf{P}(t)\mathbf{C}^T\boldsymbol{\Theta}^{-1}(t).$$

Remark 1: Notice that, even though the nominal system considers $\dot{\mathbf{b}}(t) = 0$, in the filter design the bias is assumed to be driven by zero mean, white Gaussian noise. This allows the filter to track slowly time-varying bias, in addition to variations between power-ons. The intensity of the white noise that is assumed to drive the bias is a parameter that can be fine-tuned according to the change rate of the bias.

V. Simulation Results

This section presents simulation results that were carried out prior to the experimental tests in order to assess the performance of the proposed solutions. The simulations attempt to replicate the experimental trials so that the results are comparable. The multi-position accelerometer calibration algorithm is evaluated in Section V-A, while simulation results with the proposed filtering solution for dynamic bias and gravity estimation are presented in Section V-B.

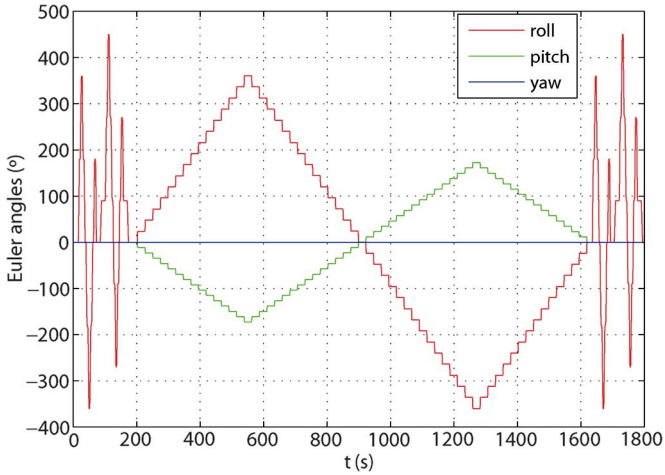

Fig. 1. Evolution of the Euler angles for accelerometer calibration.

A. Accelerometer Calibration

In order to assess the effectiveness of the proposed calibration method, Monte Carlo simulations were first carried out considering an accelerometer with

$$\mathbf{F}^{-1} = \begin{bmatrix} 0.990 & 0.001 & -0.002 \\ 0.020 & 1.005 & 0.003 \\ -0.010 & -0.004 & 1.010 \end{bmatrix}$$

$$\mathbf{b}' = \begin{bmatrix} 0.05 \\ -0.01 \\ 0.04 \end{bmatrix} (\mathrm{m/s^2})$$

and

$$\mathbf{F}_2 = 10^{-4}\mathrm{diag}(2.5, 1.5, -0.75).$$

In addition to that, sensor noise was considered. In particular, zero-mean additive white Gaussian noise was added to the acceleration measurements, with standard deviation of 0.0013 $\mathrm{m/s^2}$. In each simulation the attitude of the accelerometer varies according to Fig. 1, where the evolution of the roll, pitch, and yaw Euler angles is depicted. The corresponding evolution of the resulting gravity vector is shown in Fig. 2. As it is possible to observe, the attitude trajectory evolves in steps and covers many different configurations, not only to have the calibration problem well-posed (sufficient data) but also to achieve better results. A transition time of 2 s is used between steps and each step lasts 22 s. The data is sampled, at a sampling rate of 100 Hz, during a period of 4 s on each step, in which the accelerometer is static, for calibration purposes. The first and last periods of 180 s of the simulation are presented solely because they will be required for hardware synchronization purposes.

The resulting mean of the errors of the estimated parameters is below 10^{-9} for all variables, which evidences that the estimates are unbiased. On the other hand, the standard deviation

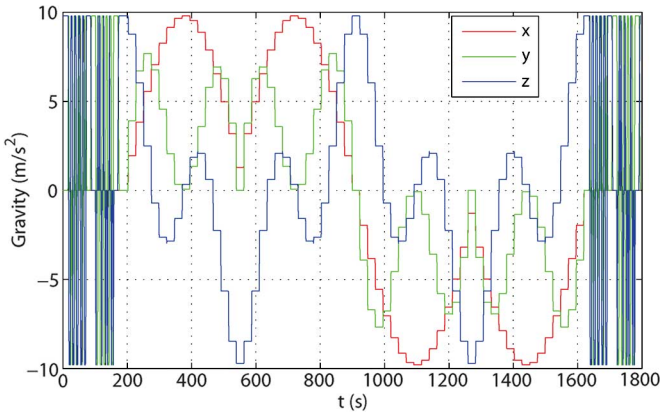

Fig. 2. Evolution of the gravity for accelerometer calibration (expressed in body-fixed coordinates).

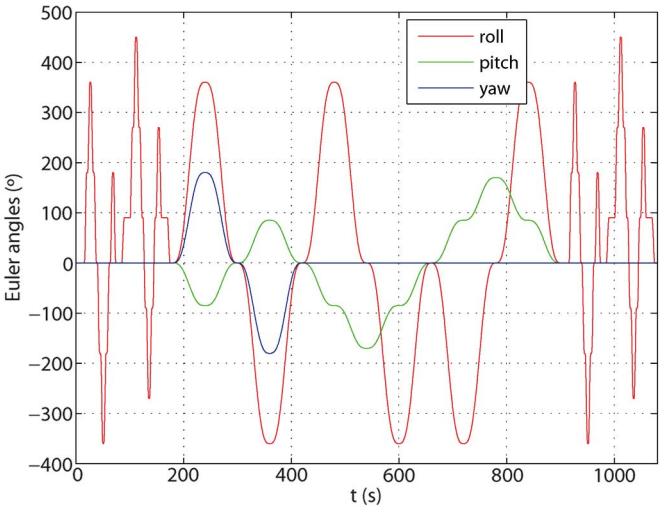

Fig. 3. Evolution of the Euler angles for dynamic bias and gravity estimation.

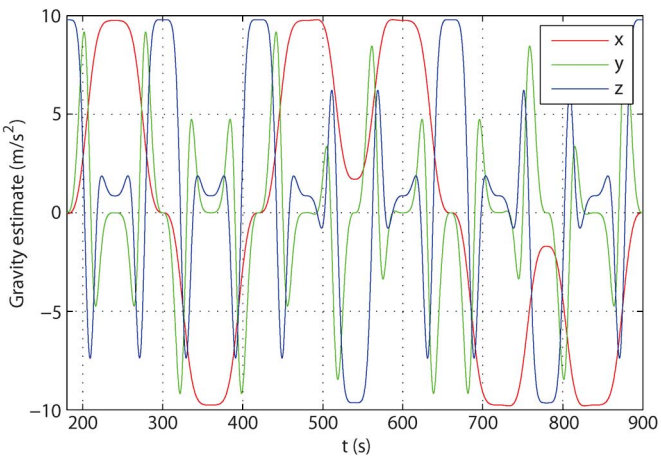

Fig. 4. Evolution of the gravity estimate (in body-fixed coordinates).

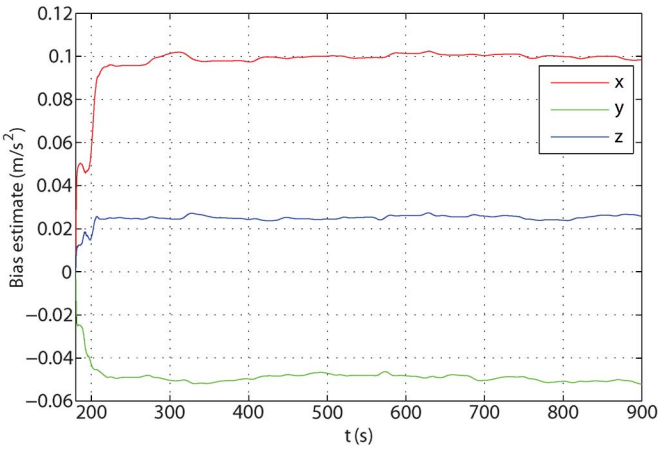

Fig. 5. Evolution of the bias estimate.

of the error stays below 10^{-7}, which corresponds to very accurate estimates of the accelerometer parameters. These values show that the proposed calibration procedure should yield good results in practice.

B. Dynamic Bias and Gravity Estimation

In order to evaluate the performance of the proposed bias and gravity estimation solution, simulations were carried out considering a setup very similar to the experimental one, which will be presented in the following section. In particular, the rotation of the accelerometer is parameterized by roll, pitch, and yaw Euler angles, whose evolution is depicted in Fig. 3.

Additive zero-mean white Gaussian noise was considered for all sensors, which were sampled at 100 Hz. The standard deviations were chosen as 0.0013 m/s^2 for the acceleration measurements, 0.05 $^\circ$/s for the angular velocity readings, and 0.01 m/s for the linear velocity measurements. In addition, the bias of the accelerometer was set to

$$\mathbf{b}' = \begin{bmatrix} 0.1 \\ -0.05 \\ 0.025 \end{bmatrix} (\text{m/s}^2).$$

The filter parameters were chosen as

$$\boldsymbol{\Xi} = \text{diag}(10^{-3}\mathbf{I}, 10^{-4}\mathbf{I}, 10^{-5}\mathbf{I})$$

and

$$\boldsymbol{\Theta} = 0.1\mathbf{I}.$$

Finally, the initial velocity and gravity estimates were set close to the true values, as the velocity is measured and the acceleration of gravity is known up to some error (the acceleration measurement is dominated by the gravity). The initial bias estimate was set to zero.

The evolution of the gravity and bias estimates are depicted in Figs. 4 and 5, respectively. As it is possible to observe, the bias converges quickly to the true values. In order to better evaluate the performance of the filter, the evolution of the errors of the linear velocity, gravity, and bias are depicted in Figs. 6–8, respectively. Clearly, the mean errors converge to zero. Moreover, the errors on the bias and gravity estimates stay well below the noise of the accelerometer, which evidences good filtering performance of the proposed solutions.

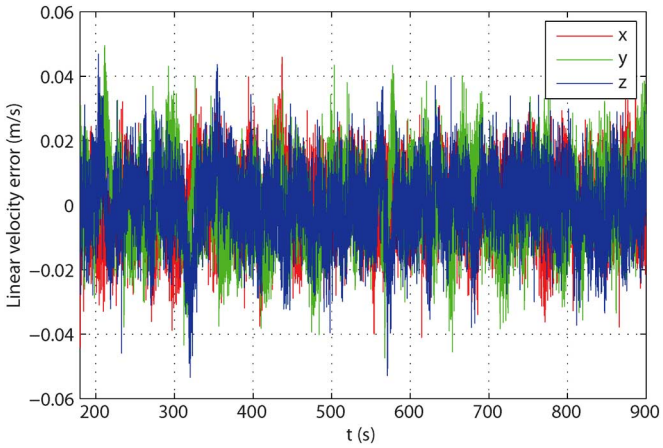

Fig. 6. Evolution of the linear velocity error.

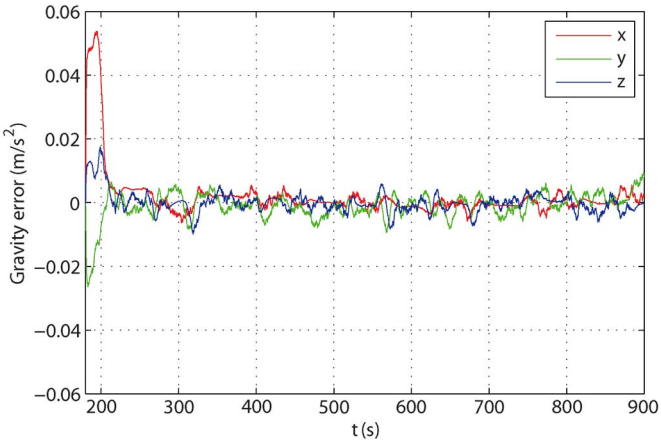

Fig. 7. Evolution of the gravity error.

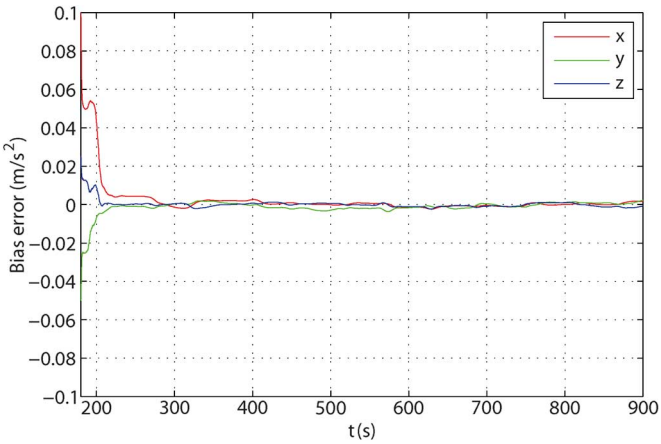

Fig. 8. Evolution of the bias error.

VI. Experimental Evaluation

Experimental tests were carried out in order to evaluate the performance of the proposed solutions. The experimental setup is detailed in Section VI-A, while the accelerometer calibration procedure and results are presented in Section VI-B. Finally, the proposed filtering solution for dynamic bias and gravity estimation is analyzed in Section VI-C.

A. Experimental Setup

To obtain high quality results, a calibration procedure requires the execution of specific maneuvers, involving the acquisition of high accuracy ground truth data to evaluate the estimated quantities produced by processing accelerometer data. The Model 2103HT from Ideal Aerosmith [21] is a three-axis MRT that provides precise angular position, rate, and acceleration for development and testing of inertial components and systems. This table, presented in Fig. 9, was used to generate the desired calibration trajectories and provide the required ground truth signals. The angular resolution of the MRT is 0.000025°. The accelerometer that was employed is presented in Fig. 10. It is a Silicon Design Inc. tri-axial analog accelerometer [22], sampled at 100 Hz using three Texas Instruments ADS1210, which are directly connected to a microcontroller board built around the Phillips XAS3 16-bit microcontroller with CAN (Controller Area Network) Bus interface [23]. The ADS1210 is a high precision, wide dynamic range, delta-sigma analog-to-digital converter (ADC), with 24-bit resolution, and it operates from a single +5 V supply. The ADS1210 differential inputs are ideal for direct connection to transducers, guaranteeing 20-bits of effective resolution, which is a suitable accuracy for the inertial sensor used in the present application. Finally, a PC104 board, connected to the CAN Bus, logs the data in a solid state disk for post-testing analysis. The table top is autonomous in terms of power and logging capabilities.

Fig. 9. Experimental setup mounted on the Ideal Aerosmith motion rate table.

B. Dynamic Accelerometer Calibration

The accelerometer unit previously introduced was subject to several tests, taken on different days and in different conditions. The calibration results show that the scale and cross-axis terms, as well as the quadratic coefficient, do not change significantly between tests, which validates the calibration of the accelerometer prior to its usage in navigation systems. However,

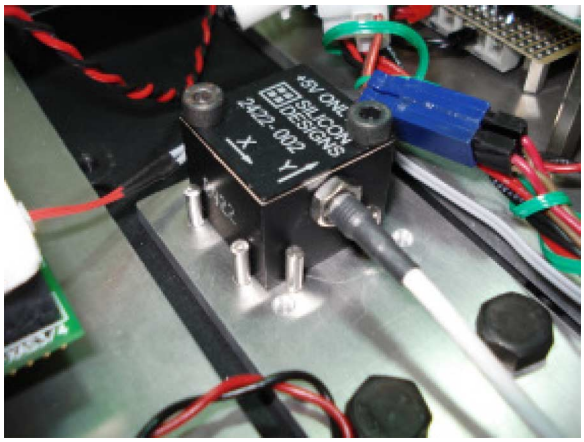

Fig. 10. Detail of the MEMS accelerometer in the experimental setup.

the bias estimates resulting from the calibration test proposed in Section III change greatly between tests, including tests where the accelerometer power was never turned off. This evidences that dynamic bias estimation is essential for this type of sensor.

The estimated parameters, which were used to correct the acceleration measurements afterwards during dynamic bias and gravity estimation, were

$$\mathbf{F}^{-1} = \begin{bmatrix} 0.9946 & 0.0037 & -0.0061 \\ -0.0091 & 0.9998 & 0.0079 \\ -0.0071 & -0.0186 & 1.0047 \end{bmatrix}$$

$$\mathbf{b}' = \begin{bmatrix} -0.7368 \\ -0.2803 \\ 0.3995 \end{bmatrix} (\mathrm{m/s}^2)$$

and

$$\mathbf{F}_2 = 10^{-4}\mathrm{diag}(-2.362, 1.055, 3.666).$$

These are all within the specifications provided by the manufacturer.

Fig. 11 presents the error between the corrected accelerometer measurements at static positions and the expected measurements, which are due only to the acceleration of gravity. It is possible to observe that, even after accelerometer calibration, the mean of the error at each position is not always zero. This is due not only to higher-order nonlinearities but also to the time-varying nature of the parameters. There exist some positions at which the standard deviation of the error is much higher. This is not due to the accelerometer but to the motion rate table, which exhibited oscillations at some positions. Finally, a vibration was detected in the outer axis of the calibration table, with a frequency around 11 Hz, which is most likely a natural resonance frequency of the body. That also contributes to the increased standard deviation of the error and it is not present in real applications. Interestingly enough, both the oscillations and the vibrations of the table are so small that a slightly lower grade accelerometer is unable to detect them.

C. Dynamic Bias and Gravity Estimation

The experimental results obtained for to dynamic bias and gravity estimation are presented in this section. The evolution of

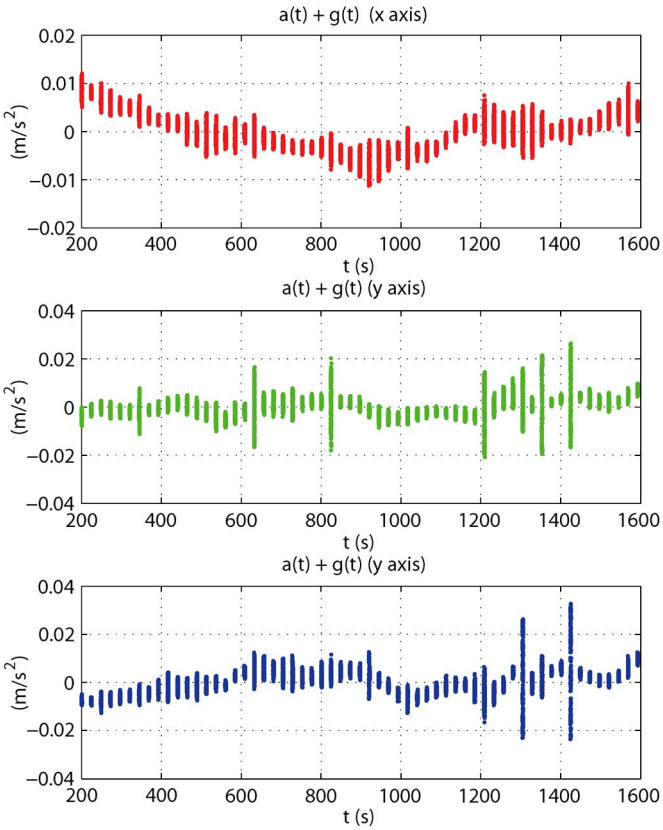

Fig. 11. Error of the accelerometer measurements after calibration correction.

the attitude is the same as the one presented in Section V-B, so that the results are comparable. The filter parameters, sampling rate, and initial estimates are also the same. Notice that, with the trajectory described in the experiment, the system dynamics for online dynamic bias and gravity estimation are uniformly completely observable, so that the Kalman filter error dynamics are globally asymptotically stable.

The evolution of the gravity and bias estimates are depicted in Figs. 12 and 13, respectively. The similarities between Figs. 12 and 4 evidence that the experimental results follow closely the simulation results. It is possible to observe that the filter keeps very good tracking of the acceleration of gravity, which is essential for attitude estimation purposes in navigation systems. It is also possible to see the time-varying nature of the bias.

Comparing the level of the accelerometer error at rest (after calibration), presented in Fig. 11, with the magnitude of the bias estimate, depicted in Fig. 13, they seem about the same for this particular unit. Nevertheless, it is important to remark that it does not render the bias estimation process useless. Indeed, any acceleration bias that is not compensated for in a navigation system leads to the degradation of the system performance, particularly due to the double integration that relates acceleration and position quantities. Moreover, it is important to stress that the bias estimate is only small in this case because the accelerometer unit had been calibrated and therefore the bias was partially compensated for, as shown in Section VI-B. Had this not been the case and the bias estimate would be very large when compared to the accelerometer noise.

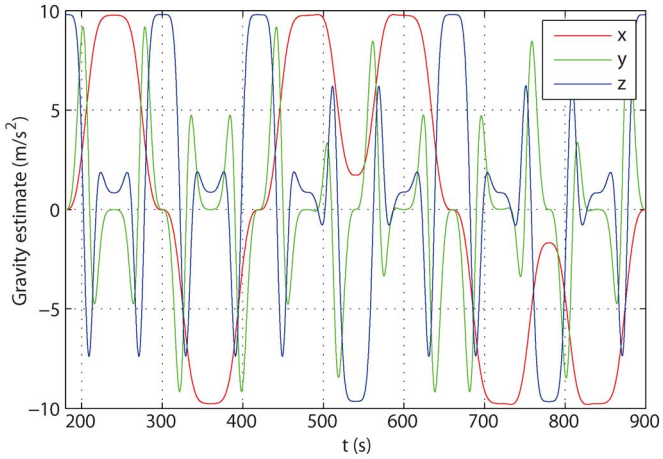

Fig. 12. Evolution of the gravity estimate (in body-fixed coordinates).

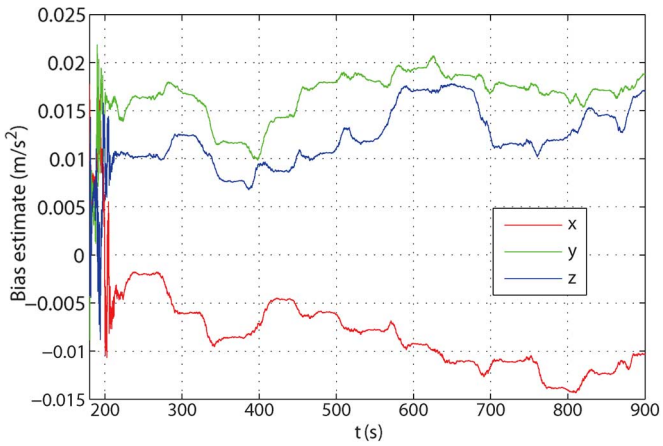

Fig. 13. Evolution of the bias estimate.

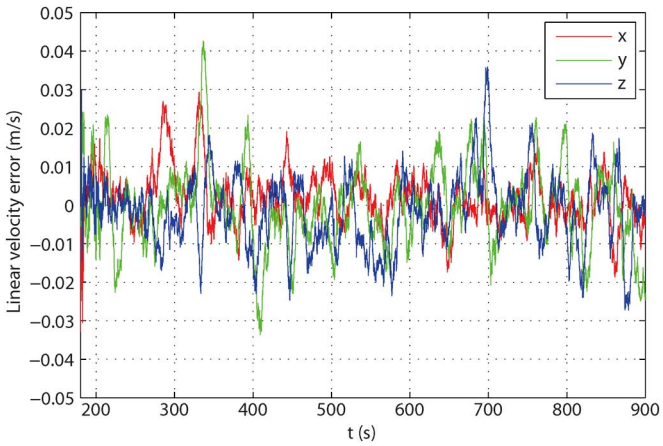

Fig. 14. Evolution of the linear velocity error.

In order to better assess the performance of the filter, the evolution of the errors of the linear velocity and gravity acceleration are depicted in Figs. 14 and 15, respectively. Clearly, the mean errors converge to zero which evidences the goodness of the proposed filtering solution.

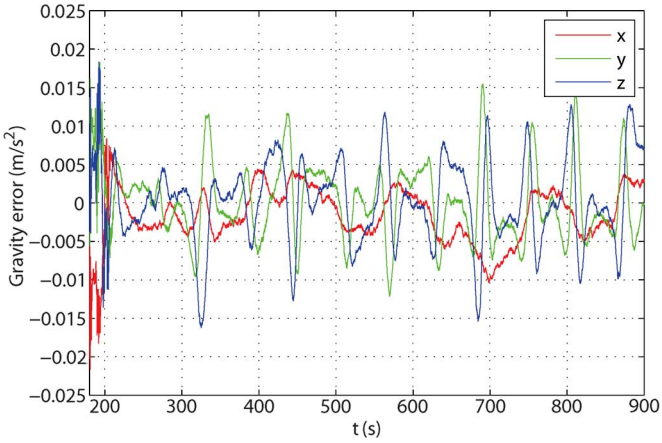

Fig. 15. Evolution of the gravity error.

VII. Conclusion

Tri-axial accelerometers are key elements in a great variety of applications and, in particular, in navigation systems. Nonidealities such as scale factors, cross coupling, and bias affect the output of these sensors, leading, in general, to prohibitive errors, particularly for sensitive and high-performance navigation systems. This justifies offline calibration as a method to overcome these nonidealities. On the other hand, these coefficients are often slowly time-varying, which renders offline calibration less effective and calls for dynamic parameter estimation. This paper presented a calibration technique for a tri-axial accelerometer and a novel dynamic filtering solution for the bias, which also accounts explicitly for the estimation of the gravity in body-fixed coordinates. Simulation results were shown that evidenced the expectable performance of the proposed algorithms. Finally, a low-cost accelerometer unit was calibrated and the bias and gravity filter was evaluated experimentally. In the tests a MRT was employed that provided ground truth signals for performance evaluation purposes, both for offline calibration and dynamic bias and gravity estimation, and that allowed to conclude that the proposed solutions exhibit excellent performance. Future work will consist in the inclusion of the proposed dynamic estimation solution in future navigation systems, previously adjusted with the calibration algorithm presented in this paper.

Acknowledgment

The authors gratefully acknowledge the expertise and contributions of L. Sebastião during the mounting process of the Ideal Aerosmith motion rate table and the help with the delogging software provided by A. Oliveira.

References

[1] R. Mahony, T. Hamel, and J.-M. Pflimlin, "Nonlinear complementary filters on the special orthogonal group," *IEEE Trans. Autom. Control*, vol. 53, no. 5, pp. 1203–1218, Jun. 2008.

[2] P. Batista, C. Silvestre, and P. Oliveira, "Sensor-based complementary globally asymptotically stable filters for attitude estimation," in *Proc. 48th IEEE Conf. Dec. Control*, 2009, pp. 7563–7568.

[3] P. Batista, C. Silvestre, and P. Oliveira, "Position and velocity optimal sensor-based navigation filters for UAVs," in *Proc. Amer. Control Conf.*, 2009, pp. 5404–5409.
[4] *IEEE Recommended Practice for Precision Centrifuge Testing of Linear Accelerometers*, IEEE Std. 836, 1991.
[5] D. Titterton and J. Weston, "Strapdown inertial navigation systems," IEE, 2004.
[6] M. Kayton and W. Fried*, Avionics Navigation Systems*. New York: Wiley, 2003.
[7] R. Rogers, "Applied mathematics in integrated navigation systems," AIAA, 2003.
[8] B. Barshan and H. Durrant-Whyte, "Inertial navigation systems for mobile robots," *IEEE Trans. Robot. Autom.*, vol. 11, no. 3, pp. 328–342, Jun. 1995.
[9] M. Grewal, V. Henderson, and R. Miyasako, "Application of Kalman filtering to the calibration and alignment of inertial navigation systems," *IEEE Trans. Autom. Control*, vol. 36, no. 1, pp. 4–13, Jan. 1991.
[10] E. Nebot and H. Durrant-Whyte, "Initial calibration and alignment of an inertial navigation," in *Proc. 4th Annu. Conf. Mechatron. Mach. Vision in Practice*, 1997, pp. 175–180.
[11] M. Stakkeland, G. Prytz, W. Booij, and S. Pedersen, "Characterization of accelerometers using nonlinear kalman filters and position feedback," *IEEE Trans. Instrum. Meas.*, vol. 56, no. 6, pp. 2698–2704, Dec. 2007.
[12] E. Renk, W. Collins, M. Rizzo, F. Lee, and D. Bernstein, "Optimization-based calibration of a triaxial accelerometer-magnetometer," in *Proc. Amer. Control Conf.*, 2005, pp. 1957–1962.
[13] N. Dumas, F. Azais, F. Mailly, A. Richardson, and P. Nouet, "A novel method for test and calibration of capacitive accelerometers with a fully electrical setup," presented at the 11th IEEE Workshop Des. Diagnostics of Electron. Circuits Syst., Bratislava, Slovakia, Apr. 2008.
[14] J. Hall and R. Williams, "Case study: Inertial measurement unit calibration platform," *J. Robot. Syst.*, vol. 17, no. 11, pp. 623–632, 2000.
[15] P. Walter, "The history of the accelerometer," *Sound Vibr.*, pp. 84–92, 2007.
[16] A. Kelly, "Modern inertial and satellite navigation systems," Robotics Inst., Carnegie Mellon Univ., Pittsburgh, PA, Tech. Rep. CMU-RI-TR-94-15, May 1994.
[17] Dept. Defense World Geodetic Syst., U.S. Dept. Defense, "World geodetic system 1984, its definition and relationships with local geodetic systems," Tech. Rep. NIMA TR8350.2, 1984.
[18] P. Batista, C. Silvestre, and P. Oliveira, "Necessary and sufficient conditions for the observability of linear motion quantities in strapdown navigation systems," in *Proc. Amer. Control Conf.*, 2009, pp. 1177–1182.
[19] R. Kalman and R. Bucy, "New results in linear filtering and prediction theory," *Trans. ASME—J. Basic Eng., Series D*, vol. 83, no. 3, pp. 95–108, Mar. 1961.
[20] , A. G. , Ed*., Applied Optimal Filtering*. Cambridge, MA: The MIT Press, 1974.
[21] Ideal Aerosmith, Inc., "2103HT multi-axis table data sheet, Rev C," 2006. [Online]. Available: http://www.ideal-aerosmith.com/
[22] Silicon Designs, Inc., "Triaxial analog accelerometer module, Model 2422," 2007. [Online]. Available: www.silicondesigns.com
[23] R. Bosch, "CAN specification version 2.0," BOSCH, 1991.

Pedro Batista (S'09) received the Licenciatura degree in electrical and computer engineering and the Ph.D. degree from Instituto Superior Técnico (IST), Lisbon, Portugal, in 2005 and 2010, respectively.

From 2004 to 2006, he was a Monitor with the Department of Mathematics, IST, and he has also received the Diploma de Mérito twice during his graduation. His research interests include sensor-based navigation and control of autonomous vehicles and he is currently a researcher at Instituto Superior Técnico/Institute for Systems and Robotics (IST/ISR).

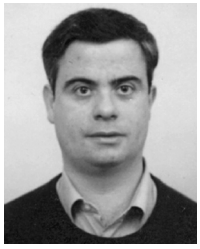

Carlos Silvestre (M'07) received the Licenciatura degree in electrical engineering, the M.Sc. degree in electrical engineering, and the Ph.D. degree in control science from the Instituto Superior Técnico (IST), Lisbon, Portugal, in 1987, 1991, and 2000, respectively.

Since 2000, he has been with the Department of Electrical Engineering, IST, where he is currently an Assistant Professor of Control and Robotics. Over the past years, he has conducted research on the subjects of vehicle and mission control of air and underwater robots. His research interests include linear and nonlinear control theory, coordinated control of multiple vehicles, gain scheduled control, integrated design of guidance and control systems, inertial navigation systems, and mission control and real time architectures for complex autonomous systems with applications to unmanned air and underwater vehicles.

Paulo Oliveira (M'92) received the Ph.D. degree from the Instituto Superior Técnico (IST), Lisbon, Portugal, in 2002.

He is an Assistant Professor with the Department of Electrical Engineering and Computers, IST, and a Researcher with the Institute for Systems and Robotics—Associated Laboratory, Lisbon, Portugal. The areas of scientific activity are robotics and autonomous vehicles with special focus on the fields of sensor fusion, navigation, positioning, and signal processing. He participated in more than 15 Portuguese and European Research projects, in the last 20 years.

Bruno Cardeira received the Licenciatura and the M.Sc. degrees in electrical engineering from the Instituto Superior Técnico (IST), Lisbon, Portugal, in 2004 and 2009, respectively.

He is currently with the Dynamical Systems and Ocean Robotics (DSOR) Laboratory, the Institute for Systems and Robotics (ISR), IST. His research interests include Strapdown Inertial Navigation Systems development, calibration and testing, and sensor fusion for autonomous vehicles.